Available online at www.sciencedirect.com
ScienceDirect
Journal of Power Sources 168 (2007) 453–458
JOURNAL OF POWER SOURCES
www.elsevier.com/locate/jpowsour

Short communication

The influence of anode gas diffusion layer on the performance of low-temperature DMFC

Jian Zhang, Ge-Ping Yin*, Qin-Zhi Lai, Zhen-Bo Wang, Ke-Di Cai, Peng Liu

Department of Applied Chemistry, Harbin Institute of Technology, Harbin 150001, PR China

Received 6 February 2007; received in revised form 8 March 2007; accepted 8 March 2007
Available online 15 March 2007

Abstract

The influence of the anode gas diffusion layers (GDLs) on the performances of low-temperature DMFCs, and the properties of mass transport and CO_2 removal on these anode GDLs were investigated. The membrane electrode assembly (MEA) based on the hydrophilic anode GDL, which consisted of the untreated carbon paper and hydrophilic anode micro-porous layer (comprised carbon black and 10 wt.% Nafion), showed the highest power density of 13.4 mW cm^{-2} at 30 °C and ambient pressure. The performances of the MEAs tended to decline with the increase of the PTFE content in the anode GDLs due to the difficulty of methanol transport. The contact angle measurements revealed that the wettabilities of the anode GDLs decreased as the increase of PTFE content. The wettabilities of the GDLs were improved by addition of hydrophilic Nafion ionomer to the GDLs. From the visualizations of CO_2 gas bubbles dynamics on the anodes using a transparent cell, it was observed that uniform CO_2 gas bubbles with smaller size formed on hydrophilic anode GDLs. And bubbles with larger size were not uniform over the hydrophobic anode GDLs. It was believed that adding PTFE to the anode GDL was not helpful for improving the CO_2 gas transport in the anode GDL of the low-temperature DMFC.

Keywords: Direct methanol fuel cell; Anode gas diffusion layer; Electrochemical impedance spectra; Flow visualization; Contact angle

1. Introduction

The direct methanol fuel cell (DMFC) has been receiving increasing attention due to its advantages of easy transportation and storage of the fuel, reduced system weight and size, high energy efficiency, and low exhaustion [1,2]. The key component of a DMFC is the membrane electrode assembly (MEA). The MEA for DMFC is usually a seven-layer structure, and it comprises a polymer electrolyte membrane, anode electrode (consisting of anode catalyst layer and anode gas diffusion layer) and cathode electrode (consisting of cathode catalyst layer and cathode gas diffusion layer) [3]. The anode gas diffusion layer (GDL) for DMFC usually consists of a backing layer, typically made of carbon paper or carbon cloth which is untreated or wet-proofed with PTFE, and a coated thin micro-porous layer (MPL) that is combined with carbon black and Nafion ionomer or PTFE.

The anode GDL serves to transport the mass and electrically connects the catalyst layer and the current collector [4]. The mass transport in the anode is a complex topic in DMFC. The liquid methanol must be transported through the anode GDL to the anode catalyst layer where it is consumed. The CO_2 gas is produced in the anode catalyst layer and must be continuously removed through the anode GDL to avoid blockage of the reaction areas. Both liquid phase transport paths and the gas phase transport paths have to be provided to reduce the polarization in the anode GDL. Several investigations were focused on the effects of anode GDLs on the performances of DMFCs. Nordlund et al. [5] and Oedegaard et al. [6] found that adding PTFE to the anode led to better gas transfer in the liquid phase and had a positive effect on the performance of DMFC. Liu et al. [7] reported that hydrophilic anode backing layer might facilitate methanol transport and resulted in better cell performance. Xu et al. [4] and Gogel et al. [8] found that the anode backing layer of a DMFC did not need to be wet-proofed with PTFE, from the viewpoint of enhancing mass transport of methanol

* Corresponding author at: P.O. Box 411#, Department of Applied Chemistry, Harbin Institute of Technology, Harbin 150001, PR China.
Tel.: +86 451 86413721; fax: +86 451 86413720.
E-mail addresses: zhangjianhit@yahoo.com.cn (J. Zhang), yingphit@hit.edu.cn (G.-P. Yin).

0378-7753/$ – see front matter © 2007 Elsevier B.V. All rights reserved.
doi:10.1016/j.jpowsour.2007.03.027

solution. Lindermeir et al. [9] compared the anode MPLs using PTFE or Nafion as binder, and found that sintering of the PTFE bonded structure improved layer properties for the management of liquid and gas transport.

However, most of the studies only considered the effects of these anode GDLs on the performances of DMFCs, there were not sufficient evidences showing the influence of these anode GDLs on the properties of mass transport and CO_2 removal in the anode of DMFCs. Moreover, most of these researches only evaluated the performances of anode GDLs of DMFCs operating at temperature higher than 60 °C. There were few papers on the effects of anode GDLs for low-temperature DMFCs (lower than 40 °C). It is not certain that whether the PTFE treatment of the anode backing layer is needed or not, and which types of the anode MPLs (hydrophilic or hydrophobic) benefit the performances of low-temperature DMFCs

The objective of this work is to investigate the influence of the anode GDLs on the performances of MEAs for low-temperature DMFCs, and the properties of mass transport and CO_2 removal on these anode GDLs. We studied the effect of PTFE content in the anode backing layer and identified the optimum PTFE or Nafion ionomer content in the anode MPL. The wettabilities of the anode GDLs were characterized by measurements of contact angles. And the CO_2 bubble behaviors on the anodes of the MEAs were observed using a transparent cell. The internal resistances and the performances of the MEAs were characterized by electrochemical impedance spectra (EIS) and polarization curves, respectively.

2. Experimental

2.1. MEA fabrication

All the electrocatalysts used in this work were prepared in-house by chemical reduction with formaldehyde of H_2PtCl_6 and $RuCl_3$ as precursors [10]. The anode catalyst was 40 wt.% Pt-Ru (with an atomic ration of 1:1)/C and the cathode catalyst was 40 wt.% Pt/C.

The home-made MEAs were the seven-layer structure, and they were fabricated by the GDL-based method [11]. Fig. 1 shows the structure of home-made seven-layer MEA. The GDLs for the cathode electrodes were wet-proofed Toray carbon papers coated with the MPLs which comprised Vulcan XC-72 carbon blacks and 20 wt.% of PTFE. The anode GDLs were the Toray carbon papers which were untreated or wet-proofed with PTFE, then coated with the MPLs which comprised Vulcan XC-72 carbon blacks and Nafion ionomer or PTFE. The various compositions of the anode GDLs of the MEAs in this paper are shown in Table 1. The loading of carbon black was 2 mg cm^{-2} for both the anode and the cathode.

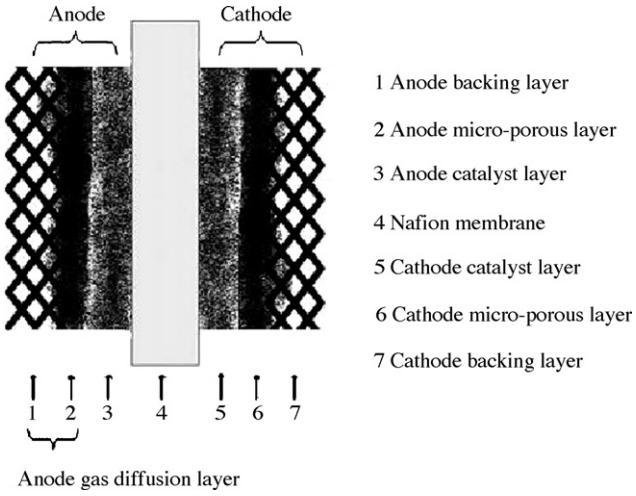

Fig. 1. The structure of home-made seven-layer MEA.

The catalyst powder and 5 wt.% Nafion ionomer solution (DuPont) were ultrasonically mixed in isopropyl alcohol to form a homogeneous catalyst ink. Then the catalyst ink was scraped onto the GDLs, and then the electrodes were dried for 2 h in the vacuum oven at 80 °C. The Nafion content in both the anode and the cathode electrodes was 20 wt.% and the metal loading (PtRu or Pt) was 2 mg cm^{-2} in each electrode.

Nafion 117 polymer membranes (DuPont) were used to fabricate MEAs. Before being applied to the electrodes, the membranes were pretreated in four steps to remove the organic and inorganic contaminants [11,12]. First, membranes were boiled in 3 wt.% H_2O_2 solution followed by washing in ultra-pure water. Then, the membranes were boiled in 0.5 mol L^{-1} H_2SO_4 solution. Finally, the membranes were boiled again in the ultra-pure water. Each step took about 1 h.

The pretreated Nafion membranes sandwiched between the anode electrodes and the cathode electrodes, and then the assemblies were hot pressed under a specific load of 100 kg cm^{-2} for 90 s at 135 °C.

Table 1
The various compositions and properties of the anode GDLs in the MEAs

MEAs	Composition of anode GDL		Highest power densities (mW cm^{-2})	Contact angle (°)
	Carbon paper	Micro-porous layer		
A1	Untreated	C + 5 wt.% Nafion	12.4	92 ± 1
A2	10 wt.% PTFE	C + 5 wt.% Nafion	11.4	129 ± 1
A3	20 wt.% PTFE	C + 5 wt.% Nafion	8.9	134 ± 1
B1	Untreated	C + 20 wt.% PTFE	10.2	152 ± 3
B2	Untreated	C + 10 wt.% PTFE	11.2	145 ± 3
B3	Untreated	C + 5 wt.% Nafion	12.8	121 ± 3
B4	Untreated	C + 10 wt.% Nafion	13.4	117 ± 3
B5	Untreated	C + 20 wt.% Nafion	12.2	110 ± 3

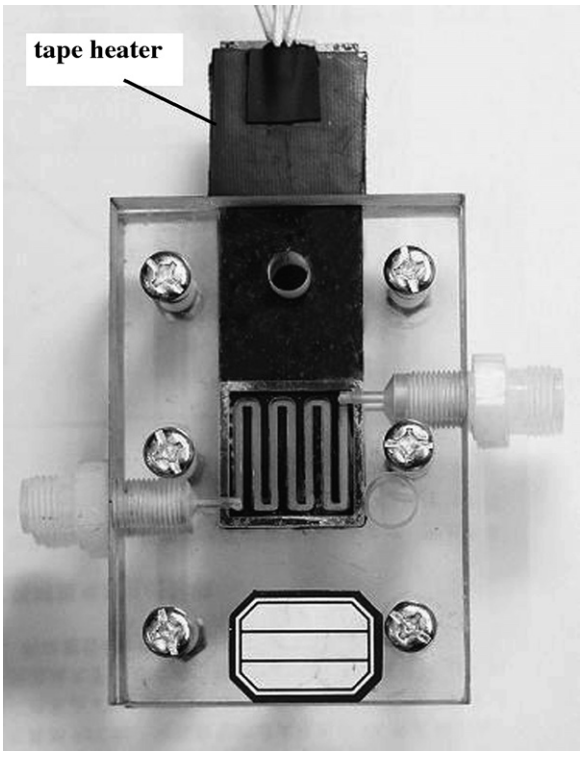

Fig. 2. The picture of the home-made transparent fuel cell.

2.2. Transparent cell

Fig. 2 shows a picture of the home-made transparent fuel cell. The cell was constructed by a pair of graphite bipolar plates mated with the plexiglass plates [13,14]. The serpentine flow channels (1.5 mm width, 2 mm depth, 2 mm rib width) were machined through the graphite bipolar plates to form an effective area of approximately 5 cm^2. The extension area of the bipolar plates served as a current collector. In addition, a tape heater was attached to the extension area to adjust the cell operating temperature to a desired value during the experiments [14]. Cell inlet and outlet manifolds were machined in the plexiglass plates. Through the transparent plexiglass plate having a thickness of 2 cm, two-phase flow characteristics of CO_2 gas and methanol solution in the anode flow field could be distinctly visualized and recorded using a Lenovo camera (ET 360) combined with a personal computer.

The electrochemical tests of these MEAs were carried out by Fuel Cell Testing System (Arbin Instrument Corp.) using the home-made transparent cell. A solution of 2 mol L^{-1} aqueous methanol solution was fed to the anode side at a flow rate of 3 mL min^{-1}. Oxygen was supplied to the cathode side at a flow rate of 200 mL min^{-1} under ambient pressure. The polarization curves of the MEAs were tested at intervals of operating time. Each point on the polarization curves represented a steady-state performance achieved after about 5 min of continuous operation at the indicated voltage. Electrochemical impedance spectra of the MEAs were measured under cell voltage at 400 mV using an electrochemical analysis instrument (model CHI 604b) in a frequency range from 10 kHz to 0.1 Hz with 6–12 points per decade at 30 °C. The amplitude of the AC-voltage was 5 mV.

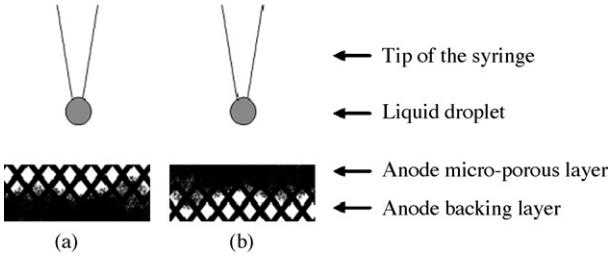

Fig. 3. The contact angle measurements on anode GDLs samples: (a) the contact angle measurements on the anode backing layers samples and (b) the contact angle measurements on the anode micro-porous layers samples.

2.3. Contact angle measurements

The contact angle measurements were performed on different anode backing layer samples and the anode MPLs samples. The contact angles were measured by the sessile-drop tests [15,16] using a contact angle system JC2000A (Zhongchen Digital Technic Apparatus Co., Ltd., China) at 25 ± 1 °C. Fig. 3a shows the contact angle measurements on the different anode backing layers samples, and Fig. 3b shows the contact angle measurements on the different anode MPLs samples. For each measurement, a 10 μL aqueous methanol solutions droplet (2 mol L^{-1}) was made by placing the tip of the syringe close to the sample surface. Then we measured the contact angle at about 15 s after the droplet attached to the sample surface. For better accuracy, measurements of contact angles were performed at five different random regions on each sample which was at least 2 cm × 2 cm and then the average value was determined.

3. Results and discussion

3.1. Contact angle analysis

The contact angle is a measurement of the wetting properties of a solid surface. It is believed that low values of contact angles indicate that the liquid spreads over, or wets the surface, while high values indicate poor wetting property. So, the wettabilities of liquid methanol solutions on the surface of anode GDLs [17–19] could be qualitatively characterized by the contact angles to a certain extent.

The contact angles of methanol solution on surfaces of anode backing layers and anode MPLs samples are shown in Fig. 4. The average values are also listed in Table 1. As shown, the untreated carbon paper exhibits the smallest contact angle. The contact angle greatly increases as the increase of PTFE amount in the backing layer, and the wettability of the anode backing layer decreases.

As shown in Fig. 4, the contact angles on the anode MPLs contained Nafion ionomer are smaller than those on the anode MPLs contained PTFE. As the contents of Nafion ionomer in the anode MPLs increase, the contact angles slightly decrease. It shows that the wettabilities of the GDLs are improved by addition of hydrophilic Nafion ionomer to the GDLs. The optimum amount of Nafion ionomer has to be determined by single-cell tests, because too much Nafion ionomer in the anode GDL may exert an adverse effect on the electrical conductivity of the GDL.

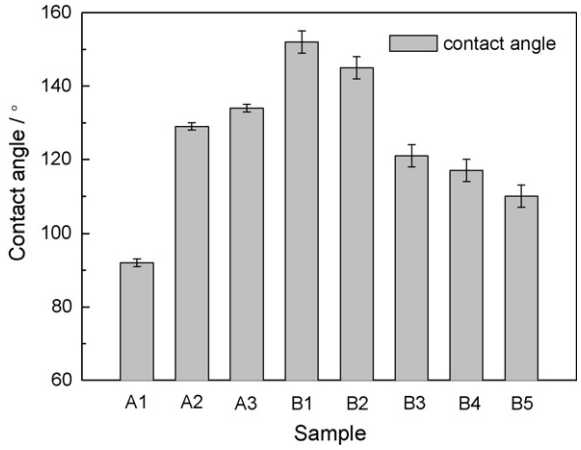

Fig. 4. The contact angles of methanol solution on surfaces of anode backing layers and anode micro-porous layers.

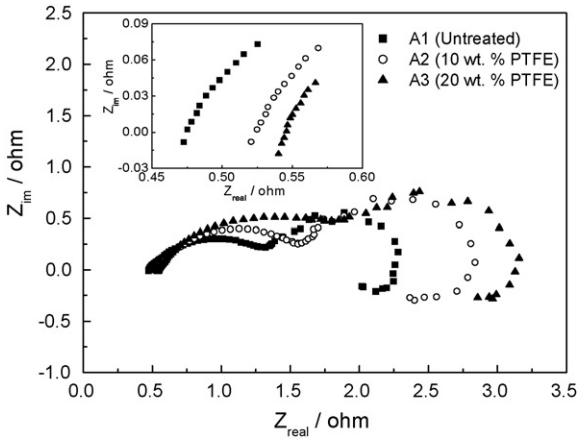

Fig. 6. Nyquist diagrams of the MEAs with different anode backing layers at 400 mV cell voltage and 30 °C.

3.2. Electrochemical characteristics of MEAs

The polarization curves and the power density curves of the MEAs with different anode backing layers are presented in Fig. 5. The cell temperature was 30 °C. The highest power densities of these MEAs are listed in Table 1. The A1 shows the highest power density of 12.4 mW cm^{-2}. The polarization curve of A2 is lower in the high current region than that of the A1, and the A3 shows a much lower performance in the high current region. It is indicated that the cell performances decrease due to the restricted mass transport in A2 and A3. The performances of the MEAs tend to decline with the increase of the PTFE content in the anode backing layers.

The EIS of the MEAs with different anode backing layers were performed at 30 °C, and the cell voltage was held at 400 mV. Nyquist diagrams of the MEAs (A1, A2 and A3) are shown in Fig. 6. In the Nyquist diagrams, pure cell resistance can be derived from the intersection of the higher frequency arc on the real axis. The cell resistance of A1 is lower than those of A2 and A3. It is believed that the carbon papers which were wet-proofed with PTFE result in an increase of cell resistances. The mass transfer resistance of the MEA can be derived in the low-frequency region from the Nyquist diagrams, and the low-frequency arc grows as the mass transfer resistance increases. The mass transfer resistance of A1 is lower than those of A2 and A3. It is believed that the PTFE treatment results in an increase of mass transfer resistance due to the difficult transport of the methanol solutions in the hydrophobic anode backing layer. These features are also consistent with the results of the contact angle analysis.

Fig. 7 shows the polarization curves and the power density curves of the MEAs with different anode MPLs. The cell temperature was 30 °C. The highest power densities of these MEAs are also listed in Table 1. The B4 shows the highest power density of 13.4 mW cm^{-2}. Fig. 7 shows that these MEAs have similar performances in the low current region. The performances of the MEAs (B3, B4, and B5) with hydrophilic anode MPLs are superior to those of the MEAs (B1, and B2) with hydrophobic anode MPLs in the high current region. It is believed that the cell performances decrease due to the restricted mass transport in the hydrophobic anode MPLs.

The EIS of the MEAs with different anode MPLs were performed at 30 °C, and the cell voltage was held at 400 mV. Nyquist diagrams of the MEAs are shown in Fig. 8. The cell resistance of

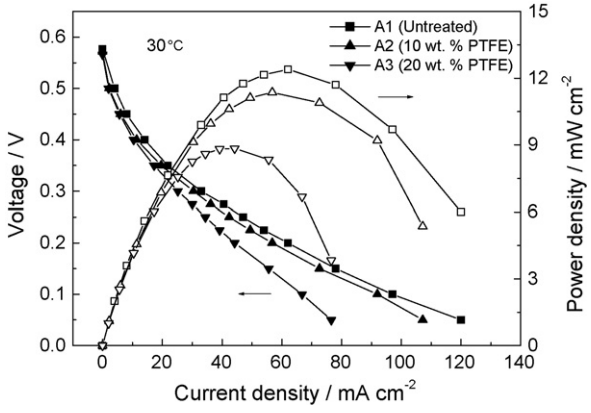

Fig. 5. The polarization curves and the power density curves of the MEAs with different anode backing layers, under application 2 mol L^{-1} methanol/oxygen, at 30 °C.

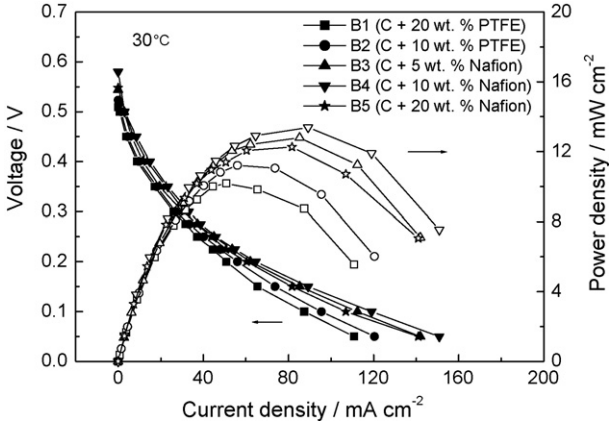

Fig. 7. The polarization curves and the power density curves of the MEAs with different anode micro-porous layers, under application 2 mol L^{-1} methanol/oxygen, at 30 °C.

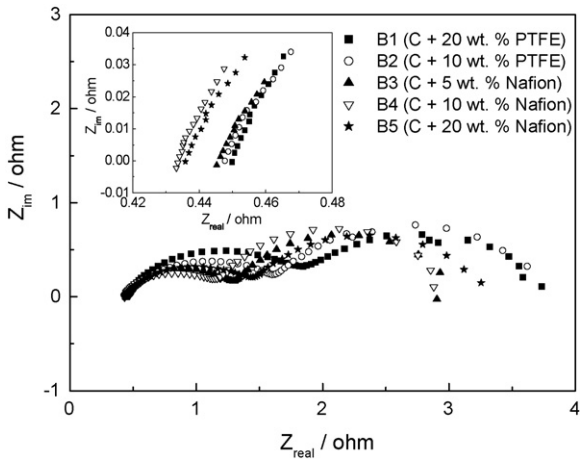

Fig. 8. Nyquist diagrams of the MEAs with different anode micro-porous layers at 400 mV cell voltage and 30 °C.

B4 is the lowest. Fig. 8 shows that the cell resistances of B4 and B5 are lower than that of the B3. There is more Nafion ionomer in the anode MPLs of B4 and B5. So, the cell resistances are lower due to the enhanced electrical contact between the anode catalyst layers and anode MPLs in B4 and B5 after the MEA hot pressing process. The cell resistances of B1 and B2 are the highest. Too much PTFE in the MPL may exert an adverse effect on the ionic or electrical conductivity of the MPL. The mass transfer resistances of B3, B4, and B5 are lower than those of B1 and B2. It is believed that the hydrophilic anode MPLs promote the mass transfer, while the hydrophobic anode MPLs increase the mass transfer resistances.

3.3. Visualization of CO_2 bubble dynamics on anode GDL

From Fig. 9, visualizations of CO_2 gas bubbles dynamics on the anodes reveal great differences between these different types of anode backing layers. For the untreated carbon paper (Fig. 9a), bubbles are produced uniformly with smaller size (about 0.1–0.5 mm in diameter, 2 mm rib width), and then they are detached easily and removed along with the flow of methanol solution. For the hydrophobic, 10 wt.% PTFE wet-proofed carbon paper (Fig. 9b), the bubbles are still very small. For the deep hydrophobic, 20 wt.% PTFE wet-proofed carbon paper (Fig. 9c), bubbles only nucleate at some certain locations, and then form large size gas slugs (about 1.0–2.0 mm) in the channel. Bubble detachment from the backing layer is significantly retarded by strong surface tension [13]. The gas bubbles occupy the flow fields, thus the diffusion of methanol is limited.

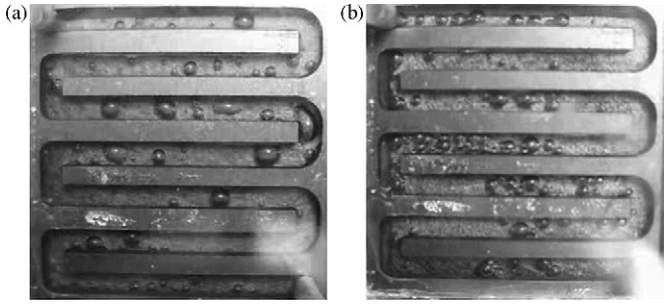

Fig. 10. Images of CO_2 bubble dynamics on the anodes with different micro-porous layers when the cell operating at 40 mA cm^{-2}, under application 2 mol L^{-1} methanol/oxygen, at 30 °C: (a) B1: carbon black and 20 wt.% PTFE and (b) B2: carbon black and 10 wt.% PTFE.

Fig. 10 compares the differences of CO_2 gas bubbles behaviors on the anode GDLs with various types of anode MPLs. For the much hydrophobic anode MPL, carbon blacks combined with 20 wt.% PTFE (Fig. 10a), bubbles nucleate at some certain locations, and then form large ones (about 0.5–2.0 mm). For the less hydrophobic anode MPL, carbon blacks combined with 10 wt.% PTFE (Fig. 10b), bubbles are smaller (about 0.5–1.5 mm) than those in B1. From the visualizations of CO_2 gas bubbles dynamics on these GDLs with various hydrophilic anode MPLs (B3, B4, and B5), it is found that small bubbles (about 0.1–0.5 mm) are formed uniformly, and there are no obvious differences between them. Fig. 9a shows the CO_2 gas bubbles behaviors on the GDL with hydrophilic anode MPL.

For the hydrophilic anode GDL with smaller contact angle, the methanol solution may transport through the anode GDL to the catalyst layer uniformly and easily, thus the CO_2 bubbles are produced uniformly. The bubbles form and grow to a small size, and then detach easily due to weak surface tension on the hydrophilic GDL [20]. After departing from the surface of the GDL, gas bubbles travel upwards to the upper surface of the channel due to buoyancy, and move towards the outlet of the flow field with liquid methanol solution.

For the hydrophobic anode GDL, there are more hydrophobic pores which enhance the gas transport. However, many hydrophobic surface pores are probably blocked or sealed with the liquid phase in the anode of DMFC due to the liquid fuel methanol. Hence, there are only a limited number of hydrophilic open channels serve as methanol solution transport paths and

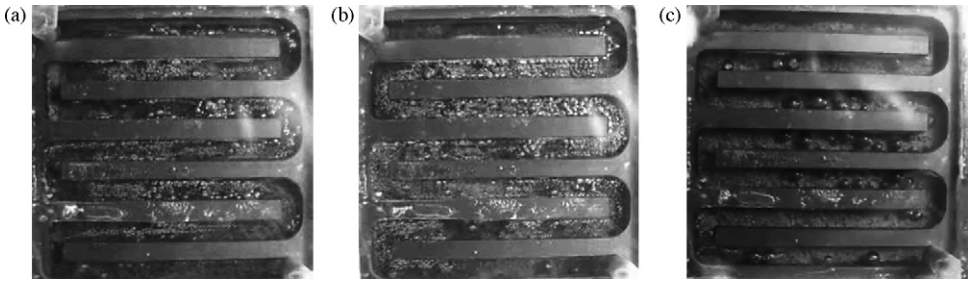

Fig. 9. Images of CO_2 bubble dynamics on the anodes with different backing layers when the cell operating at 40 mA cm^{-2}, under application 2 mol L^{-1} methanol/oxygen, at 30 °C: (a) A1: untreated; (b) A2: 10 wt.% PTFE and (c) A3: 20 wt.% PTFE.

carbon dioxide removal paths. This means that the methanol solution has to diffuse through some certain paths into the reaction sites and the CO_2 gas bubbles have to accumulate in the GDL and form relatively large bubbles until they find an open channel for removal away from the inside of the GDL [20]. Large gas slugs are formed and attached on the surface of anode GDL, and block the channel. Thus, the methanol diffusion and local generation of CO_2 bubbles is reduced, and then the performance of the MEA decreases.

4. Conclusion

We have investigated the influence of the anode GDLs on the performances of low-temperature DMFCs and the properties of mass transport and CO_2 removal on these anode GDLs. The contact angles on the anode GDLs increase as the amount of PTFE increased, and the wettabilities of the anode GDLs decrease. The wettabilities of the GDLs are improved by addition of hydrophilic Nafion ionomer to the GDLs. The performances of the MEAs tend to decline with the increase of the PTFE content in the anode GDLs. The MEAs with hydrophilic anode MPLs exhibit superior performances to the MEAs with hydrophobic anode MPLs due to the lower mass transfer resistances. The MEA based on the hydrophilic anode GDL, which consisted of the untreated carbon paper and hydrophilic anode MPL (comprised carbon blacks and 10 wt.% Nafion), shows the highest power density of 13.4 mW cm^{-2} at 30 °C and ambient pressure.

Moreover, from the visualizations of CO_2 gas bubbles dynamics on the anodes, it is demonstrated that uniform CO_2 gas bubbles with smaller size formed on hydrophilic anode GDLs. And bubbles with larger size are not uniform over the hydrophobic anode GDLs. It is believed that adding PTFE to the anode GDL is not helpful for improving the CO_2 gas transport in the anode GDL of the low-temperature DMFC.

Acknowledgements

This work was supported by Natural Science Foundation of China (No. 20476020 and No. 20606007).

References

[1] M. Baldauf, W. Preidel, J. Power Sources 84 (1999) 161.
[2] Z.B. Wang, G.P. Yin, P.F. Shi, J. Electrochem. Soc. 152 (2005) A2406.
[3] S. Litster, G. Mclean, J. Power Sources 130 (2004) 61.
[4] C. Xu, T.S. Zhao, Q. Ye, Electrochim. Acta 51 (2006) 5524.
[5] J. Nordlund, A. Roessler, G. Lindbergh, J. Appl. Electrochem. 32 (2002) 259.
[6] A. Oedegaard, C. Hebling, A. Schmitz, S. Moller-Holst, R. Tunold, J. Power Sources 127 (2004) 187.
[7] J.G. Liu, G.Q. Sun, F.L. Zhao, G.X. Wang, G. Zhao, L.K. Chen, B.L. Yi, Q. Xin, J. Power Sources 133 (2004) 175.
[8] V. Gogel, T. Frey, Y.S. Zhu, K.A. Friedrich, L. Jorissen, J. Garche, J. Power Sources 127 (2004) 172.
[9] A. Lindermeir, G. Rosenthal, U. Kunz, U. Hoffmann, J. Power Sources 129 (2004) 180.
[10] Z.B. Wang, G.P. Yin, P.F. Shi, Carbon 44 (2006) 133.
[11] J. Zhang, G.P. Yin, Z.B. Wang, Y.Y. Shao, J. Power Sources 160 (2006) 1035.
[12] Y.Y. Shao, G.P. Yin, Y.Z. Gao, Chin. J. Inorg. Chem. 21 (2005) 1060.
[13] P. Argyropoulos, K. Scott, W.M. Taama, Electrochim. Acta 44 (1999) 3575.
[14] H. Yang, T.S. Zhao, Q. Ye, J. Power Sources 139 (2005) 79.
[15] H.M. Yu, C. Ziegler, M. Oszcipok, M. Zobel, C. Hebling, Electrochim. Acta 51 (2006) 1199.
[16] U.H. Jung, K.T. Park, E.H. Park, S.H. Kim, J. Power Sources 159 (2006) 529.
[17] C. Lim, C.Y. Wang, Electrochim. Acta 49 (2004) 4149.
[18] V. Gurau, M.J. Bluemle, E.S. De Castro, Y.M. Tsou, J.A. Mann, T.A. Zawodzinski, J. Power Sources 160 (2006) 1156.
[19] E.C. Kumbur, K.V. Sharp, M.M. Mench, J. Power Sources 161 (2006) 333.
[20] P. Argyropoulos, K. Scott, W.M. Taama, J. Appl. Electrochem. 29 (1999) 661.